Inorganic Chemistry

Article

pubs.acs.org/IC

Substituent Effects on Spin State in a Series of Mononuclear Manganese(III) Complexes with Hexadentate Schiff-Base Ligands

Brendan Gildea,[†] Michelle M. Harris,[†] Laurence C. Gavin,[†] Caroline A. Murray,[†] Yannick Ortin,[†] Helge Müller-Bunz,[†] Charles J. Harding,[‡] Yanhua Lan,[§] Annie K. Powell,[†,§] and Grace G. Morgan*[,†]

[†]School of Chemistry and Chemical Biology, University College Dublin, Belfield, Dublin, D4 Ireland

[‡]Department of Chemistry, The Open University, Walton Hall, Milton Keynes, MK7 6AA U.K.

[§]Institut für Anorganische Chemie, Universität Karlsruhe, Physikhochhaus Wolfgang-Gaede-Str. 1, Karlsruhe, D-76128 Germany

Supporting Information

ABSTRACT: Eleven new mononuclear manganese(III) complexes prepared from two hexadentate ligands, L1 and L2, with different degrees of steric bulk in the substituents are reported. L1 and L2 are Schiff bases resulting from condensation of *N*,*N*′-bis(3-aminopropyl)ethylenediamine with 3-methoxy-2-hydroxybenzaldehyde and 3-ethoxy-2-hydroxybenzaldehyde respectively, and are members of a ligand series we have abbreviated as R-Sal$_2$323 to indicate the 323 alkyl connectivity in the starting tetraamine and the substitution (R) on the phenolate ring. L1 hosts a methoxy substituent on both phenolate rings, while L2 bears a larger ethoxy group in the same position. Structural and magnetic properties are reported in comparison with those of a previously reported analogue with L1, namely, [MnL1]NO$_3$, (**1e**). The BPh_4^- and PF_6^- complexes [MnL1]BPh$_4$, (**1a**), [MnL2]BPh$_4$, (**2a**), [MnL1]PF$_6$, (**1b**′), and [MnL2]-PF$_6$, (**2b**), with both ligands L1 and L2, remain high-spin (HS) over the measured temperature range. However, the monohydrate of (**1b**′) [MnL1]PF$_6$·H$_2$O, (**1b**), shows gradual spin-crossover (SCO), as do the ClO_4^-, BF_4^-, and NO_3^- complexes [MnL1]ClO$_4$·H$_2$O, (**1c**), [MnL2]ClO$_4$, (**2c**), [MnL1]BF$_4$·H$_2$O, (**1d**), [MnL2]BF$_4$·0.4H$_2$O, (**2d**), [MnL1]NO$_3$, (**1e**), and [MnL2]NO$_3$·EtOH, (**2e**). The three complexes formed with ethoxy-substituted ligand L2 all show a higher $T_{1/2}$ than the analogous complexes with methoxy-substituted ligand L1. Analysis of distortion parameters shows that complexes formed with the bulkier ligand L2 exhibit more deformation from perfect octahedral geometry, leading to a higher $T_{1/2}$ in the SCO examples, where $T_{1/2}$ is the temperature where the spin state is 50% high spin and 50% low spin. Spin state assignment in the solid state is shown to be solvate-dependent for complexes (**1b**) and (**2e**), and room temperature UV−visible and NMR spectra indicate a solution-state spin assignment intermediate between fully HS and fully low spin in 10 complexes, (**1a**)−(**1e**) and (**2a**)−(**2e**).

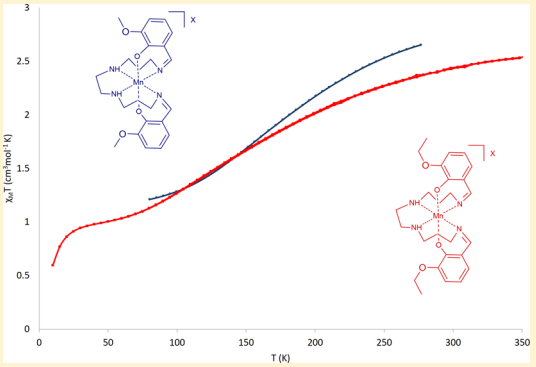

INTRODUCTION

The spin-crossover (SCO) phenomenon is an example of molecular bistability that has been extensively studied[1] due to its potential for technological applications[2,3] as a result of changes to physical properties such as magnetic moment,[1] color,[1,3] dielectric constant,[4] or electrical resistance,[5] to list a few. The transition between the low-spin (LS) ground state to the high-spin (HS) metastable state can be triggered by varying temperature,[6,7] pressure,[8−13] or magnetic field[14−17] or by exposure to irradiation using the light-induced excited spin-state trapping effect (LIESST).[18−21] SCO can also be induced by the nuclear-decay induced excited spin-state trapping (NIESST)[22] and hard X-ray induced excited spin-state trapping (HAXIESST)[23] effects, but these techniques are less commonly employed. Although the SCO phenomenon is theoretically possible for octahedral d^4−d^7 ions and the square planar d^8 configuration,[24−26] it is mostly observed in octahedral Fe(II)[6,27−30] and Fe(III)[31−34] complexes and to a lesser extent those of Co(II).[35−38] SCO in octahedral d^4 ions such as Cr(II)[39] and Mn(III)[40] has been reported, but until very recently was considered to be exceptional. We have now established that ligands of the R-Sal$_2$323 series (323 indicates the 323 alkyl connectivity in the starting tetraamine and the substitution (R) on the phenolate ring), Scheme 1, can promote the SCO effect in Mn(III),[41−46] and the resulting complex series offer great potential for changing the d^4 spin state.[47,48] This can be achieved through changing the charge-balancing anion, while keeping the complex cation constant,[43] or by changing the ligand substituents.[44] To date we have examined the effect of changing only the anion[43] and/or minor changes to the ligand within a small set of anions.[44] Although no clear pattern has as yet emerged, it is clear that the spin state of Mn(III) complexes in these series is very sensitive to solid-state lattice contents. A systematic study of a family of related Mn(III) compounds may aid in elucidating the importance of crystal engineering in determining SCO profile and in modulation of $T_{1/2}$,[43,44] as has been achieved for several

Received: February 6, 2014
Published: June 5, 2014

   dx.doi.org/10.1021/ic5003012 | *Inorg. Chem.* 2014, 53, 6022−6033

Scheme 1. Synthesis of Complexes [MnL1]X and [MnL2]X, with R−Sal$_2$323 Ligands L1 and L2

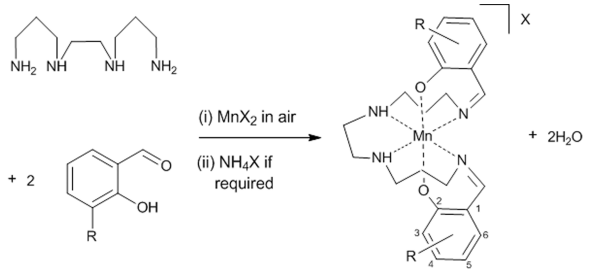

[MnL1]BPh$_4$	(1a)	[MnL2]BPh$_4$	(2a)
[MnL1]PF$_6$·H$_2$O	(1b)	[MnL2]PF$_6$	(2b)
[MnL1]ClO$_4$·H$_2$O	(1c)	[MnL2]ClO$_4$	(2c)
[MnL1]BF$_4$·H$_2$O	(1d)	[MnL2]BF$_4$·0.41H$_2$O	(2d)
[MnL1]NO$_3$	(1e)	[MnL2]NO$_3$·EtOH	(2e)

Fe(II),[49−54] Fe(III),[55−59] and Co(II)[60,61] SCO series. Structural relationships are also important factors in characterizing SCO complexes, leading to an understanding of spin-state preferences.[62−64] We have shown the effect of raising $T_{1/2}$ by increasing alkyl chain lengths on the phenolate ring on the SCO behavior of Fe(III) salts in solution.[65] Here we now report a comparative study on the solid-state magnetic behavior, bond lengths, and distortion parameters for two sets of complexes with common anions prepared with closely related 3-OMe (L1) and 3-OEt (L2) substituted ligands. Our aim is to examine the effect of methodically changing a remote substituent on the ligand while keeping the anion constant, to try and ascertain the relative influence of ligand and anion in determining the choice of electronic state in this most interesting coordination environment. Complexes of the $[MnL1]^+$ and $[MnL2]^+$ cations were each isolated as BPh_4^-, PF_6^-, BF_4^-, and ClO_4^- salts, and $[MnL2]^+$ was also isolated as the NO_3^- salt for comparison with the previously reported NO_3^- salt of $[MnL1]^+$.[41] Solvated complexes were recovered in several cases, and loss of solvent resulted in a change of spin state in at least two instances. Spin state in solution media was also investigated for all 10 complexes at room temperature and was found to be intermediate between HS and LS in all cases.

RESULTS AND DISCUSSION

The synthesis of Mn(III) complexes with R-Sal$_2$323 (R = 3-OMe or 3-OEt) ligands is a facile reaction, achieved in this case by the Schiff base condensation reaction of *N*,*N*′-bis(3-aminopropyl)-ethylenediamine with 2 equiv of R-salicylaldehyde, addition of hydrated manganese(II) perchlorate or nitrate, followed by the addition of an ammonium salt of the required anion as appropriate, Scheme 1.

Slow evaporation of the filtered acetonitrile/alcohol reaction mixture yielded dark brown crystals of all 10 complexes (**1a**)−(**2e′**). All were characterized by elemental analysis, IR, UV−vis (vis = visible), and Faraday or SQUID magnetometry, Table 1. Several of the complexes with L1 and L2 crystallized with a solvate molecule, Table 1. The complexes all showed a characteristic C═N stretch between 1616−1623 cm^{-1}, confirming formation of the Schiff base and a vibration associated with the appropriate counterion X, Table 1.

Magnetic Characterization of Mn(III) Complexes. Susceptibility data on ground samples of the complexes with the 3-OMe substituted ligand L1 (**1a**)−(**1e**) were collected on a Faraday balance, in warming mode only between 80 K and high temperature, with the exception of (**1b**). In light of the dependence of the spin state on solvent content in some cases, it is preferable to measure crystalline samples, and the variable-temperature magnetic susceptibility $\chi_M T$ for crystalline samples of the 3-OEt series L2 (**2a**)−(**2e**) and complex (**1b**) was recorded on a Quantum Design MPMSXL-SQUID magnetometer, usually in both cooling and warming modes, over a variety of temperature ranges between 10 and 350 K. The plots of $\chi_M T$ versus temperature for (**1a**)−(**2e**) are shown in Figure 1, where a range of magnetic responses is obvious.

Complexes with BPh_4^- counterion, (**1a**) and (**2a**) persist in the HS state over the measured temperature range with values close to the expected spin-only value of $\chi_M T$ = 3 cm^3 mol^{-1} K for an S = 2 electronic state.[66] Stabilization of the HS state by BPh_4^- counterions has previously been observed in Fe(III) Schiff-base complexes, where the BF_4^- and ClO_4^- salts of the same cation exhibit SCO.[56] The PF_6^- complex, (**1b**), with L1 initially crystallized as a monohydrate that exhibits SCO between 10 and 300 K, Figure 1. However, loss of water over time results in the

Table 1. Magnetic and Spectroscopic Characterization of (1a)−(2e′)

	IR (cm^{-1})	$\chi_M T$		$\chi_M T$	$T_{1/2}$	ε (M^{-1} cm^{-1}) in CH$_3$CN	
	C═N, X[a]	(cm^3 mol^{-1} K)		(cm^3 mol^{-1} K)	(K)		
		at 80 K	at 280 K	at 298 K in CD$_3$CN		λ_{max} (nm): 370−400	λ_{max} (nm): 280−300
[MnL1]BPh$_4$, (**1a**)	1621, 1467	2.93	3.06	1.89	HS	2840	20 000
[MnL2]BPh$_4$, (**2a**)	1619, 1462	2.95	2.99	2.09	HS	7600	35 610
[MnL1]PF$_6$·H$_2$O, (**1b**)	1616, 850	0.93	1.93	2.13	300	6360	23 640
[MnL1]PF$_6$, (**1b′**)[b]		2.82	2.83				
[MnL2]PF$_6$, (**2b**)	1618, 843	3.03	3.08	1.99	HS	5120	18 660
[MnL1]ClO$_4$·H$_2$O, (**1c**)	1618, 1078	1.15	2.68	2.13	192	2670	10 610
[MnL2]ClO$_4$, (**2c**)	1619, 1076	1.15	2.42	2.36	196	6880	26 160
[MnL1]BF$_4$·H$_2$O, (**1d**)	1623, 1098	1.21	2.65	1.84	181	4670	21 350
[MnL2]BF$_4$·0.4H$_2$O, (**2d**)	1621, 1080	1.13	2.38	2.89	197	3980	16 830
[MnL1]NO$_3$, (**1e**)	1618, 1384	1.01	2.29[41]	1.77	249	2440	9 830
[MnL2]NO$_3$·EtOH, (**2e**)	1621, 1381	1.21	2.02	2.61	277	4620	17 370
[MnL2]NO$_3$·0.6EtOH, (**2e′**)[c]					HS		

[a]X = counterion. [b][MnL1]PF6 (**1b′**) was recovered after dehydration of analogue [MnL1]PF$_6$·H$_2$O, (**1b**), and its magnetic properties are reported here for comparison with (**1b**). [c]Loss of solvation in (**2e**) resulted in (**2e′**) as revealed by a second structural determination some months later. Only structural data are reported here from which it was clear that the complex was HS.

dx.doi.org/10.1021/ic5003012 | Inorg. Chem. 2014, 53, 6022−6033

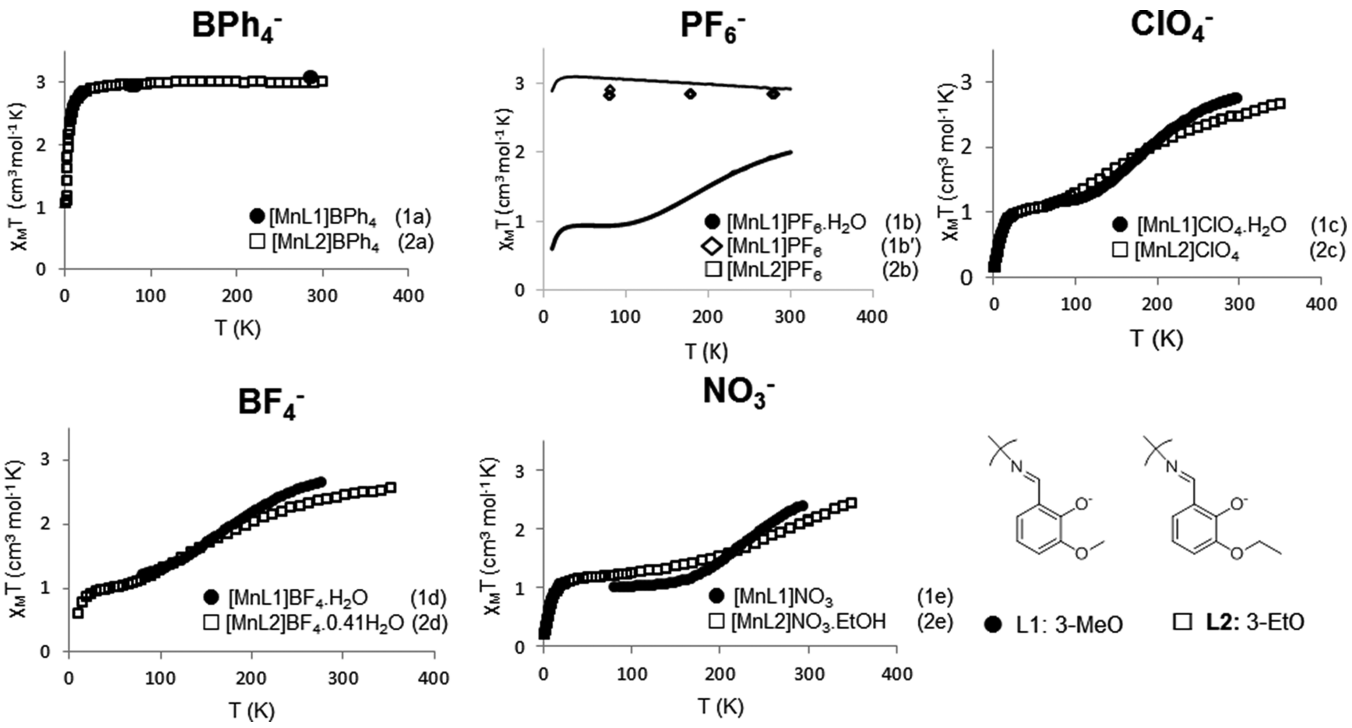

Figure 1. Plots of $\chi_M T$ versus temperature for Mn(III) complexes (**1a**)−(**1e**), (**1b**′), and (**2a**)−(**2e**).

dehydrated analogue (**1b**′), which is HS over the same temperature range. At 20 K the remaining ClO_4^-, BF_4^-, and NO_3^- complexes with L1 and L2 are all low spin (LS), with values of $\chi_M T$ close to 1 cm^3 mol^{-1} K as expected for an $S = 1$ electronic state.[66] Below 15 K significant zero-field splitting causes a sharp decrease from the expected spin-only value of $\chi_M T$ = 1 cm^3 mol^{-1} K for $S = 1$. On warming the six Mn(III) complexes with ClO_4^-, (**1c**) and (**2c**), BF_4^-, (**1d**) and (**2d**), and NO_3^-, (**1e**)[41] and (**2e**), counterions, pronounced but incomplete SCO is shown. The ClO_4^-complexes (**1c**) and (**2c**) have similar SCO profiles above 80 K, although that of (**2c**) is slightly more gradual. The BF_4^- complexes, (**1d**) and (**2d**), also undergo SCO above 80 K with $T_{1/2}$ values of 181 and 197 K, Table 1. The nitrate complexes, (**1e**)[41] and (**2e**), start to switch from LS to HS at approximately 140 and 60 K, with $T_{1/2}$ values of 249 and 277 K, respectively. It is interesting to note that the general effect of adding an extra CH_2 group to the phenol group substituent, from OMe to OEt, is to increase $T_{1/2}$. This could be important in attempting to design an SCO complex with a $T_{1/2}$ at room temperature for device applications.

Variable-Temperature Single-Crystal X-ray Crystallography. Dark brown-black crystals for each complex were recovered on standing in air and were structurally characterized by single-crystal diffraction, Table 2. Three of the complexes with L1, (**1b**), (**1c**), and (**1d**), and two of the complexes with L2, (**2d**) and (**2e**), crystallize as solvates. The emphasis of the structural studies was on (i) bond length changes and (ii) supramolecular interactions to try and elucidate if these influence the choice of spin state. Magnetostructural correlations were also examined using the changes in local distortion parameters (Σ and Θ)[62] that accompany the spin-state change.

The local geometry around each Mn(III) ion is pseudo-octahedral with two *trans*-phenolate donors, two *cis*-amine donors, and two *cis*-imine donors. Complexes (**1e**)[41] and (**2b**) both have a 2-fold rotation axis through the Mn center, which bisects the ethylene linkage between the two amine nitrogen atoms to generate geometrically equivalent pairs of *cis*-imine, *cis*-amine, and *trans*-phenolate donors. Complex (**2e**) crystallizes as an ethanol solvate, which was structurally characterized at 100 K. A second data set was collected at 293 K after several months, which revealed a loss of solvent resulting in a complex that now contained 0.6 EtOH molecules, thereby ruling out a meaningful comparison of the two structures in terms of bond length changes that accompany SCO. From the X-ray determinations, it is possible to calculate the distortion around the Mn(III) ion and to examine the magneto-structural correlation.

Bond Length Changes. We have previously shown that Mn(III) complexes from the R-Sal$_2$323 series undergo an equatorial elongation upon SCO from LS to HS by comparison of the bond lengths of the complexes at high and low temperatures.[41−44] The most striking feature is the significant elongation of all four Mn−N bond lengths in sharp contrast to the Mn−O bond lengths, which remain unchanged. This structural change could be interpreted as corresponding to accommodation of the Jahn−Teller distortion by population of the antibonding $d_{x^2-y^2}$ orbital in the Mn−N_4 plane upon switching to the HS state. The spin state of the metal can generally be inferred using the generally observed ranges shown in Table 3.

The bond lengths of all SCO complexes (**1b**), (**1c**), (**2c**), (**1d**), (**1e**),[41] and (**2d**) were measured at two temperatures, namely, 100 and 293 K. All SCO complexes show an increase in Mn−N_{imine} (N1 and N4) and Mn−N_{amine} (N2 and N3) distances on warming, Table 4 and Figure 2, but no significant change to the Mn−O_{phen} lengths.

Distortion Parameters. Analysis of octahedral distortion can be achieved by quantifying the angular distortion[62] with Θ and Σ. These parameters were applied to a series of Fe(II) SCO complexes in the [Fe(II)Ln(NCS)$_2$] series discussed by Guionneau in 2004.[63] This was expanded in 2008 by Halcrow to investigate Fe(III) systems with Sal$_2$trien.[64] A third parameter

dx.doi.org/10.1021/ic5003012 | Inorg. Chem. 2014, 53, 6022−6033

Table 2. Crystallographic Data for (1a)−(2e)

	[MnL1]BPh_4, **1a**	[MnL2]BPh_4, **2a**	[MnL1]PF_6 ·H_2O, **1b**	[MnL1]PF_6 ·H_2O, **1b**	[MnL2]PF_6, **2b**	[MnL1]ClO_4 ·H_2O, **1c**	[MnL1]ClO_4 ·H_2O, **1c**	[MnL2]ClO_4, **2c**	[MnL2]ClO_4, **2c**
	100 K	100 K	100 K	293 K	100 K	100 K	293 K	100 K	293 K
formula	$C_{48}H_{52}BN_4O_4Mn$	$C_{50}H_{56}BN_4O_4Mn$	$C_{24}H_{34}N_4O_5F_6PMn$	$C_{24}H_{34}N_4O_5F_6PMn$	$C_{26}H_{36}N_4O_4F_6PMn$	$C_{24}H_{34}N_4O_9ClMn$	$C_{24}H_{34}N_4O_9ClMn$	$C_{26}H_{36}N_4O_8ClMn$	$C_{26}H_{36}N_4O_8ClMn$
molecular weight	814.69	842.74	658.46	658.46	668.50	612.94	612.94	622.98	622.98
crystal size (mm)	0.25 × 0.20 × 0.20	0.29 × 0.20 × 0.17	1.00 × 0.20 × 0.20	0.60 × 0.60 × 0.10	0.23 × 0.12 × 0.09	0.60 × 0.50 × 0.50	1.00 × 0.60 × 0.20	0.18 × 0.14 × 0.12	0.50 × 0.40 × 0.40
crystal system	triclinic	triclinic	monoclinic	monoclinic	orthorhombic	monoclinic	monoclinic	monoclinic	monoclinic
space group	$P\bar{1}$ (#2)	$P\bar{1}$ (#2)	$P2_1/c$ (#14)	$P2_1/c$ (#14)	$Pba2$ (#32)	$P2_1/c$ (#14)	$P2_1/n$ (#14)	Pn (#7)	Pn (#7)
a, b, c (Å)	a = 11.4458(12)	a = 13.2597(3)	a = 7.8766(7)	a = 8.0615(10)	a = 11.3441(2)	a = 7.7836(9)	a = 8.0428(14)	a = 7.4950(2)	a = 7.7747(8)
	b = 14.0220(15)	b = 13.3988(2)	b = 20.5438(18)	b = 20.789(3)	b = 16.9530(3)	b = 20.491(3)	b = 20.504(3)	b = 11.0996(2)	b = 11.1398(12)
	c = 14.2813(15)	c = 13.7821(3)	c = 16.8393(15)	c = 17.047(2)	c = 7.7231(1)	c = 16.519(2)	c = 16.737(3)	c = 17.1219(5)	c = 17.1389(18)
α, β, γ (deg)	α = 67.556(3)	α = 75.886(2)	α = 90	α = 90	α = 90	α = 90°	α = 90°	α = 90°	α = 90
	β = 77.817(3)	β = 85.042(2)	β = 101.5440(10)	β = 102.722(2)	β = 90	β = 100.267(2)	β = 101.818(3)	β = 102.300(2)	β = 102.839(2)
	γ = 71.090(3)	γ = 66.494(2)	γ = 90	γ = 90	γ = 90	γ = 90	γ = 90	γ = 90	γ = 90
volume (Å^3)	1994.1(4)	2177.45(8)	2669.7(4)	2786.9(6)	1485.28(4)	2592.5(5)	2701.5(8)	1391.70(6)	1447.3(3)
Z	2	2	4	4	2	4	4	2	2
Dc(calcd) (mg/m^3)	1.357	1.285	1.638	1.569	1.495	1.570	1.507	1.487	1.430
μ (mm^{-1})	0.383	0.353	0.641	0.614	0.575	0.674	0.646	0.626	0.602
F(000)	860	892	1360	1360	692	1280	1280	652	652
collected refns	14 951	57 313	22 139	21 331	15 983	23 578	23 493	14 671	26 257
independent refns	6409	10 986	6200	5468	3716	6214	5471	6228	6290
	[R(int) = 0.0482]	[R(int) = 0.0339]	[R(int) = 0.0249]	[R(int) = 0.0260]	[R(int) = 0.0300]	[R(int) = 0.0226]	[R(int) = 0.0263]	[R(int) = 0.0238]	[R(int) = 0.0166]
R_1 [$I > 2\sigma(I)$]	$R1$ = 0.0519	$R1$ = 0.0360	$R1$ = 0.0335	$R1$ = 0.0421	$R1$ = 0.0267	R_1 = 0.0350	R_1 = 0.0415	$R1$ = 0.0279	$R1$ = 0.0285
	w$R2$ = 0.1256	w$R2$ = 0.0783	w$R2$ = 0.0822	w$R2$ = 0.1075	w$R2$ = 0.0543	wR_2 = 0.0902	wR_2 = 0.1154	w$R2$ = 0.0653	w$R2$ = 0.0763

	[MnL1]BF_4 ·H_2O, **1d**	[MnL1]BF_4 ·H_2O, **1d**	[MnL2]BF_4 ·0.4H_2O, **2d**	[MnL2]BF_4 ·0.4H_2O, **2d**	[MnL1]NO_3, **1e**[41]	[MnL1]NO_3, **1e**[41]	[MnL2]NO_3 ·EtOH, **2e**	[MnL2]NO_3·0.6EtOH, **2e′**
	100 K	293 K	100 K	293 K	100 K	293 K	100 K	293 K
formula	$C_{24}H_{34}BN_4O_5F_4Mn$	$C_{24}H_{34}BN_4O_5F_4Mn$	$C_{26}H_{36.84}BN_4O_{4.42}F_4Mn$	$C_{26}H_{36.80}BN_4O_{4.40}F_4Mn$	$C_{24}H_{32}N_5O_7Mn$	$C_{24}H_{32}N_5O_7Mn$	$C_{28}H_{42}N_5O_8Mn$	$C_{27.26}H_{39.78}N_5O_{7.63}Mn$
molecular weight	600.30	600.30	617.94	617.45	557.49	557.49	631.61	614.56
crystal size (mm)	0.27 × 0.21 × 0.17	0.40 × 0.20 × 0.02	0.60 × 0.50 × 0.02	0.30 × 0.23 × 0.07	0.50 × 0.40 × 0.20	0.50 × 0.40 × 0.20	0.80 × 0.60 × 0.03	0.25 × 0.13 × 0.09
crystal system	monoclinic	monoclinic	monoclinic	monoclinic	orthorhombic	orthorhombic	monoclinic	monoclinic
space group	$P2_1/c$ (#14)	$P2_1/c$ (#14)	Pn (#7)	$P2_1/n$ (#7)	$Pccn$ (#56)	$Pccn$ (#56)	$P2_1/c$ (#14)	$P2_1/c$ (#14)
a, b, c (Å)	a = 7.73110(7)	a = 8.003(3)	a = 7.5994(6)	a = 7.8039(1)	a = 17.8374(12)	a = 17.833(2)	a = 8.2733(5)	a = 8.4972(4)
	b = 20.4412(2)	b = 20.451(8)	b = 10.9479(8)	b = 11.0456(2)	b = 8.4113(6)	b = 8.9144(12)	b = 22.3068(14)	b = 22.4305(9)
	c = 16.5760(2)	c = 16.825(7)	c = 17.1061(13)	c = 17.2003(2)	c = 16.8132(12)	c = 16.504(2)	c = 16.7509(10)	c = 16.8324(7)
α, β, γ (deg)	α = 90	α = 90	α = 90	α = 90	α = 90	α = 90	α = 90	α = 90
	β = 100.2191(8)	β = 101.798(8)	β = 102.808(1)	β = 103.052(2)	β = 90	β = 90	β = 103.998(1)	β = 102.706(4)
	γ = 90	γ = 90	γ = 90	γ = 90	γ = 90	γ = 90	γ = 90	γ = 90
volume (Å^3)	2578.00(5)	2695.7(18)	1387.77(18)	1444.34(4)	2522.6(3)	2623.65	2999.6(3)	3129.6(2)

dx.doi.org/10.1021/ic5003012 | Inorg. Chem. 2014, 53, 6022−6033

Table 2. continued

	[MnL1]BF_4·H_2O, **1d** 100 K	[MnL1]BF_4·H_2O, **1d** 293 K	[MnL2]BF_4·0.4H_2O, **2d** 100 K	[MnL2]BF_4·0.4H_2O, **2d** 293 K	[MnL1]NO_3, **1e**[41] 100 K	[MnL1]NO_3, **1e**[41] 293 K	[MnL2]NO_3·EtOH, **2e** 100 K	[MnL2]NO_3·0.6EtOH, **2e′** 293 K
Z	4	4	2	2	4	4	4	4
Dc(calcd) (mg/m^3)	1.547	1.479	1.479	1.420	1.468	1.411	1.399	1.304
μ (mm^{-1})	4.814	0.560	0.544	0.523	0.577	0.555	0.497	0.473
F(000)	1248	1248	644.1	644	1168	1168	1336	1284
collected refns	27 252	14 408	15 561	29 094	20 136	17 576	26 279	16 541
independent refns	5399	3303	7961	5889	3078	2314	6146	3815
	[R(int) = 0.0265]	[R(int) = 0.0553]	[R(int) = 0.0198]	[R(int) = 0.0212]	[R(int) = 0.0223]	[R(int) = 0.0274]	[R(int) = 0.0397]	[R(int) = 0.0465]
R_1 [$I > 2\sigma(I)$]	$R1$ = 0.0323	$R1$ = 0.0647	$R1$ = 0.0396	$R1$ = 0.0273	$R1$ = 0.0303	$R1$ = 0.0480	$R1$ = 0.0439	$R1$ = 0.0475
	w$R2$ = 0.0848	w$R2$ = 0.1584	w$R2$ = 0.0965	w$R2$ = 0.0711	w$R2$ = 0.0799	w$R2$ = 0.0886	w$R2$ = 0.1069	w$R2$ = 0.1327

Table 3. Average Bond Lengths (Å) for Both HS and LS Mn(III) Complexes in the R-Sal$_2$323 Series[41−44]

	LS	HS
Mn−O_{phen}	1.8−1.9	1.8−1.9
Mn−N_{imine}	1.9−2.0	2.0−2.1
Mn−N_{amine}	2.0−2.1	2.2−2.3

to consider is α, which Halcrow defined as the dihedral angle between the least-squares planes of the two phenolate rings in complexes of the related Sal$_2$trien series. It should also be possible to apply these distortion parameters to Mn(III) SCO complexes of the R-Sal$_2$323 series and compare with those of the first Mn(III) SCO complex reported by Sim and Sinn in 1981.[40] Their complex with the tripodal trianionic ligand pyrol tren had Θ values of 240° and 199° in the HS and LS states, respectively, while the change in Σ was small, with values of 71° and 64° in the HS and LS states, respectively. Here distortion parameters have been calculated at low and high temperatures, Table 5, for most of the Mn(III) complexes in an effort to relate the degree of distortion with spin-state preference.

In general, the HS state of a complex is more distorted from a perfect octahedron than is the LS state, due to population of antibonding orbitals. For the SCO complexes, (**1b**)−(**2d**), the values of Σ, Θ, and α are higher in the HS state than those of the LS state. All three distortion parameters are higher for complexes at the same temperature containing ligand L2 than L1. Guionneau has shown that it is possible to show a correlation between $T_{1/2}$ and $\Delta\Theta$.[67] He suggests that, for SCO complexes of the type [Fe(NCS)$_2$L$_2$], a higher $\Delta\Theta$ leads to a greater structural rearrangement of the lattice during SCO, disfavoring the transition. This extra unfavorable lattice energy would have to be overcome by supercooling the sample, leading to an observed inverse dependence of $T_{1/2}$ on $\Delta\Theta$. However, upon examination of the correlation of $\Delta\Theta$ and $T_{1/2}$ for the SCO complexes (**1c**)−(**2e**) for our Mn(III) series, inverse dependence is not observed, and a plot of $T_{1/2}$ versus $\Delta\Theta$, Figure 3, reveals no obvious relationship in the case of Mn(III).

One possible reason for the difference in trend between Fe(II) and Mn(III) SCO complexes is the fact that Mn(III) shows a strong Jahn−Teller effect in the HS state. This is generally manifested as a lengthening of bonds in only four of the donors in manganese complexes of R-Sal$_2$323 ligands upon population of an antibonding orbital in the HS state, rather than all six donors as is typical for Fe(II) SCO complexes.

Intermolecular Interactions. It was also of interest to look for temperature-dependent changes in hydrogen bonding or $\pi-\pi$ interactions that might align with SCO. Neither of the HS tetraphenylborate complexes [MnL1]BPh_4, (**1a**), and [MnL2]-BPh_4, (**2a**), crystallized with solvation, and no hydrogen bonding or other intermolecular interactions were detected, Figure 4.

In contrast, two different packing arrangements were observed in the PF_6^- salts, [MnL1]PF_6·H_2O, (**1b**), and [MnL2]PF_6, (**2b**). Of these two only (**1b**) with the methoxy-substituted ligand (L1) shows any hydrogen-bonding interactions at 100 K. The disordered PF_6^- counterion forms a hydrogen bond to the water solvent molecule, which also hydrogen bonds to the phenolate oxygen donor. The loss of the water solvent molecule to form (**1b′**) results in a HS state, possibly due to the disruption of this hydrogen bonding interaction on dehydration. The disorder in the PF_6^- ion was modeled as dynamic rotation around the equatorial plane, where each fluorine atom was modeled in four equatorial positions in a "spinning top" arrangement, Figure 5.

dx.doi.org/10.1021/ic5003012 | Inorg. Chem. 2014, 53, 6022−6033

Table 4. Selected Bond Lengths for [MnL1]X and [MnL2]X (Å)

bond lengths of Mn(III) complexes (Å)									
	1a	**2a**	**1b**	**1b**	**2b**	**1c**	**1c**	**2c**	**2c**
	100 K	100 K	100 K	293 K	100 K	100 K	293 K	100 K	293 K
	$[MnL1]BPh_4$	$[MnL2]BPh_4$	$[MnL1]PF_6{\cdot}H_2O$	$[MnL1]PF_6{\cdot}H_2O$	$[MnL2]PF_6$	$[MnL1]ClO_4{\cdot}H_2O$	$[MnL1]ClO_4{\cdot}H_2O$	$[MnL2]ClO_4$	$[MnL2]ClO_4$
	HS	HS	LS	HS	HS	LS	HS	LS	HS
$Mn-O_{phen}$	1.8829(18)	1.8586(10)	1.8784(11)	1.8775(15)	1.8639(9)	1.8755(11)	1.8710(14)	1.8835(13)	1.8810(12)
	1.8516(18)	1.8687(10)	1.8847(11)	1.8742(15)		1.8866(11)	1.8755(15)	1.8706(14)	1.8662(13)
$Mn-N_{im}$	2.065(2)	2.0950(11)	1.9913(13)	2.098(2)	2.1063(13)	1.9890(14)	2.0538(18)	1.9940(17)	2.0483(16)
	2.135(2)	2.1294(12)	2.0084(14)	2.0430(19)		1.9987(14)	2.104(2)	2.011(2)	2.0948(18)
$Mn-N_{am}$	2.233(2)	2.2086(12)	2.0603(14)	2.166(2)	2.2333(15)	2.0589(14)	2.162(2)	2.0775(17)	2.1604(17)
	2.256(2)	2.2479(12)	2.0638(14)	2.142(2)		2.0583(15)	2.173(2)	2.0742(19)	2.1861(19)
	1d	**1d**	**2d**	**2d**	**1e**[41]	**1e**[41]	**2e**[a]	**2e′**[a]	
	100 K	293 K	100 K	293 K	100 K	293 K	100 K	293 K	
	$[MnL1]BF_4{\cdot}H_2O$	$[MnL1]BF_4{\cdot}H_2O$	$[MnL2]BF_4{\cdot}0.4H_2O$	$[MnL2]BF_4{\cdot}0.4H_2O$	$[MnL1]NO_3$	$[MnL1]NO_3$	$[MnL2]NO_3{\cdot}EtOH$	$[MnL2]NO_3{\cdot}0.6EtOH$	
	LS	HS	LS	HS	LS	HS	HS	HS	
$Mn-O_{(phen)}$	1.8769(10)	1.875(4)	1.8825(14)	1.8816(14)	1.8719(9)	1.868(1)	1.8726(13)	1.879(2)	
	1.8896(10)	1.879(4)	1.8767(15)	1.8704(15)			1.8629(14)	1.867(3)	
$Mn-N_{(im)}$	1.9961(13)	2.064(5)	1.9913(18)	2.0435(19)	1.9883(11)	2.072(2)	2.0668(17)	2.075(3)	
	2.0073(13)	2.107(5)	2.019(2)	2.102(2)			2.1385(17)	2.126(3)	
$Mn-N_{(am)}$	2.0677(13)	2.177(5)	2.0757(19)	2.148(2)	2.0501(11)	2.161(2)	2.1916(17)	2.184(3)	
	2.0704(13)	2.190(5)	2.094(2)	2.193(2)			2.2440(17)	2.227(3)	

[a]Loss of solvation in (**2e**) resulted in (**2e′**) as revealed by a second structural determination some months later.

dx.doi.org/10.1021/ic5003012 | Inorg. Chem. 2014, 53, 6022−6033

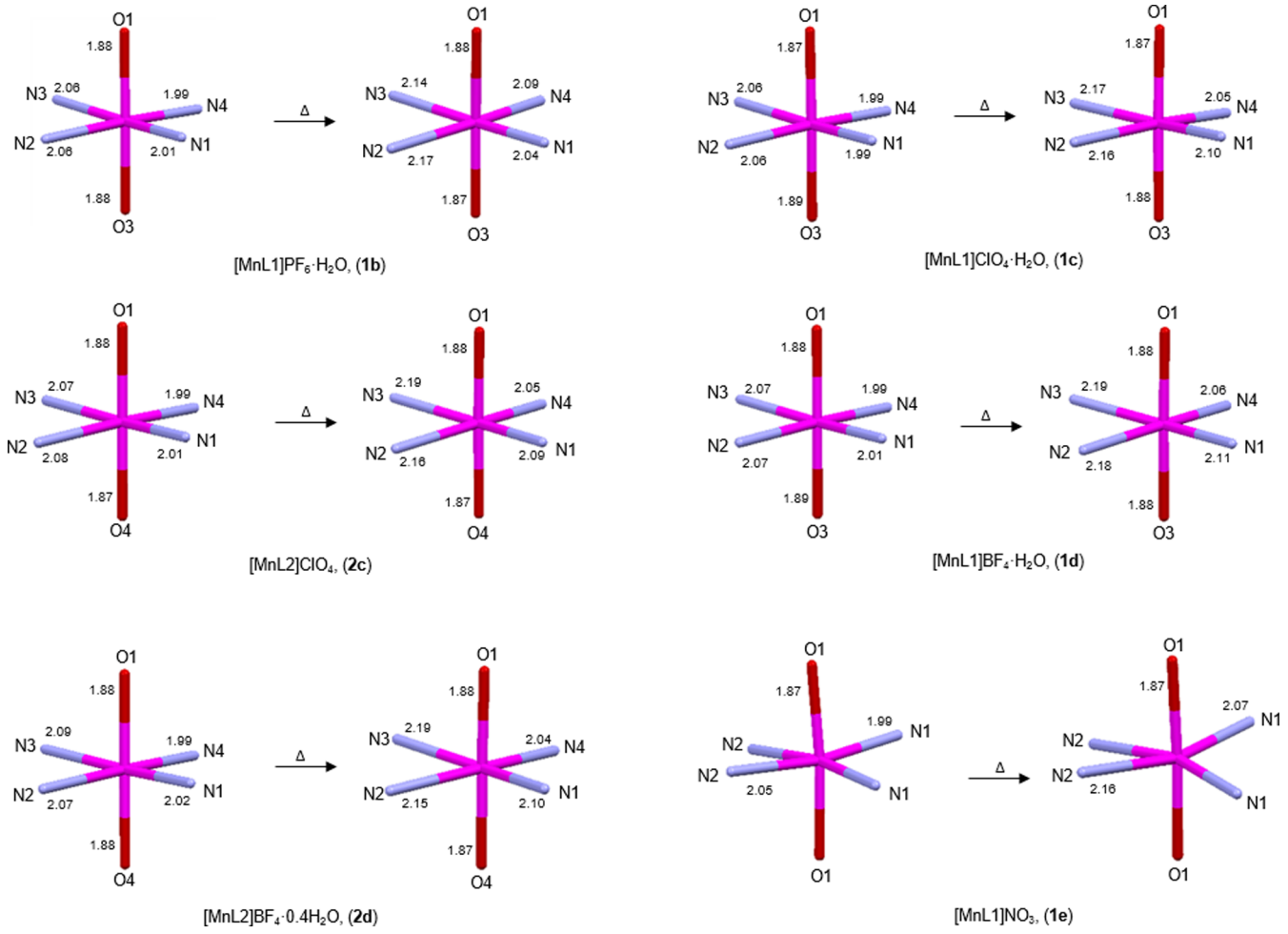

Figure 2. Immediate coordination sphere of the SCO complexes showing the change in Mn−donor bond lengths on warming for complexes (**1b**), (**1c**), (**2c**), (**1d**), (**2d**), and (**1e**).[41] Bond lengths are rounded to hundredths; for accurate bond lengths with standard deviations, see Table 4

Table 5. Distortion Parameters for Mn(III) Complexes (1a)−(1e), (1b′), and (2a)−(2e′)

	100 K			293 K			suggested
	Σ (deg)[c]	Θ (deg)[d]	α (deg)[e]	Σ (deg)	Θ (deg)	α (deg)	spin state
[MnL1]BPh_4, (**1a**)	78.1	220.9	73.0				HS
[MnL2]BPh_4, (**2a**)	70.2	182.2	64.9				HS
[MnL1]PF_6·H_2O, (**1b**)[a]	31.9	84.9	40.6	44.9	131.8	42.0	solvate-dependent SCO
[MnL2]PF_6, (**2b**)	75.9	92.7	58.2				HS
[MnL1]ClO_4·H_2O, (**1c**)	32.8	84.4	42.3	48.1	140.1	44.1	SCO
[MnL2]ClO_4, (**2c**)	33.9	95.1	50.9	51.3	145.0	54.1	SCO
[MnL1]BF_4·H_2O, (**1d**)	32.8	87.2	41.9	49.1	143.5	44.1	SCO
[MnL2]BF_4·0.4H_2O, (**2d**)	34.4	97.3	53.4	51.2	145.0	55.1	SCO
[MnL1]NO_3, (**1e**)[41]	45.0	104.0	73.0	70.7	169.7	80.5	SCO
[MnL2]NO_3·EtOH, (**2e**)[b]	67.0	199.1	64.4				solvate-dependent SCO
[MnL2]NO_3·0.6EtOH, (**2e′**)[b]				68.0	190.6	68.4	HS

[a][MnL1]PF_6·H_2O, (**1b**), lost solvent over time, but structural data collected at 100 and 293 K in close succession is for the hydrated SCO complex, Table 2. [b]Loss of solvation in [MnL2]NO_3·EtOH, (**2e**), resulted in (**2e′**) as revealed by a second structural determination at 293 K some months later. Bond length data and distortion parameters suggest both complexes are HS, in contrast to the magnetic data, which show SCO. [c]Σ is a measure of the local angular distortion in the octahedral donor set quantified by taking the sum of the distortion from 90° for each of the D−M−D′ angles. [d]Θ is the sum of the deviation of the rectangular faces from 60°. [e]α is the dihedral angle between the least-squares planes of the two phenolate rings.

This dynamic disorder in the PF_6^- counterion persisted upon heating (**1b**) to 293 K. Complex (**2b**) exhibits no intermolecular interactions at 100 K.

Comparison of intermolecular interactions in SCO complexes (**1c**) and (**2c**), (**1d**) and (**2d**), and (**1e**) and (**2e**):

Perchlorate complex [MnL1]ClO_4, (**1c**), contains a water solvate molecule, whereas the ethoxy analogue [MnL2]ClO_4, (**2c**), crystallizes without solvation, and intermolecular interactions are different in each. The presence of water in (**1c**) allows for hydrogen bonding from the ClO_4^- counterion to the water

dx.doi.org/10.1021/ic5003012 | Inorg. Chem. 2014, 53, 6022−6033

solvate molecule, which in turn hydrogen bonds to the phenolate oxygen donor, O_{phen}, Figure 6.

The hydrogen bonding in (**1c**) remains upon heating the complex to room temperature, despite the fact that (**1c**) undergoes SCO in this temperature range. This may be because there is little change in the Mn−O_{phen} distances during SCO. The ethoxy-substituted complex (**2c**) does not contain any hydrogen-bonding interactions, possibly due to the lack of a potential hydrogen-bonding solvate within the unit cell, but the SCO profile is similar to that of (**1c**), indicating that intermolecular interactions are not a dominant factor in this case.

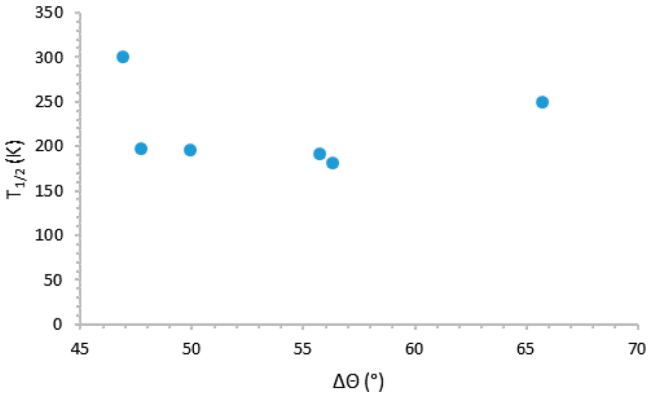

Figure 3. Plot of $T_{1/2}$ and the change in the degree of trigonal distortion of the coordination sphere ΔΘ between 100 and 293 K for SCO complexes (**1b**), (**1c**), (**2c**), (**1d**), (**2d**), and (**1e**).

The BF_4^- salts [MnL1]BF_4·H_2O, (**1d**), and [MnL2]BF_4·0.4H_2O, (**2d**), have different degrees of hydration and different hydrogen-bonding connectivity. The methoxy-substituted complex, (**1d**), crystallizes with one water solvate molecule and at 100 K forms discrete intermolecular hydrogen-bonding interactions between the BF_4^- anion and the water solvate and from the water to the phenolate oxygen donor, O_{phen}, which persist to 293 K, Figure 7. This hydrogen-bonding motif remains even as the complex undergoes SCO, and similar arguments can be applied as for (**1c**).

The ethoxy-substituted complex (**2d**) crystallized with only a fraction (0.4%) of water solvate molecule per complex and also shows a discrete arrangement of intermolecular hydrogen-bonding interactions between the BF_4^- anion and the water solvate and in this case from the water to the oxygen of the ethoxy substituent, Figure 7. This is the only complex of the series to

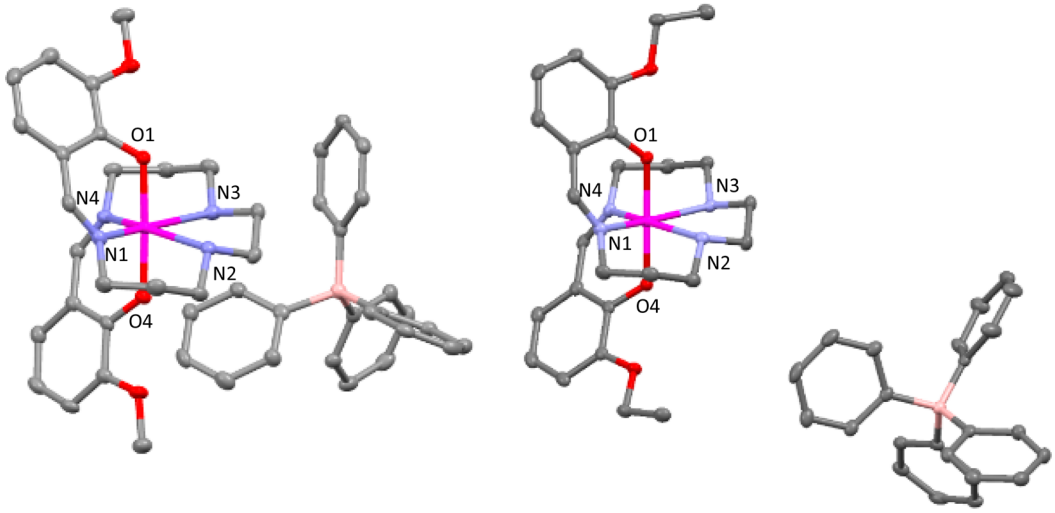

Figure 4. Relative orientation of cation and anion in [MnL1]BPh_4, (**1a**) (left) and [MnL2]BPh_4, (**2a**) (right) at 100 K.

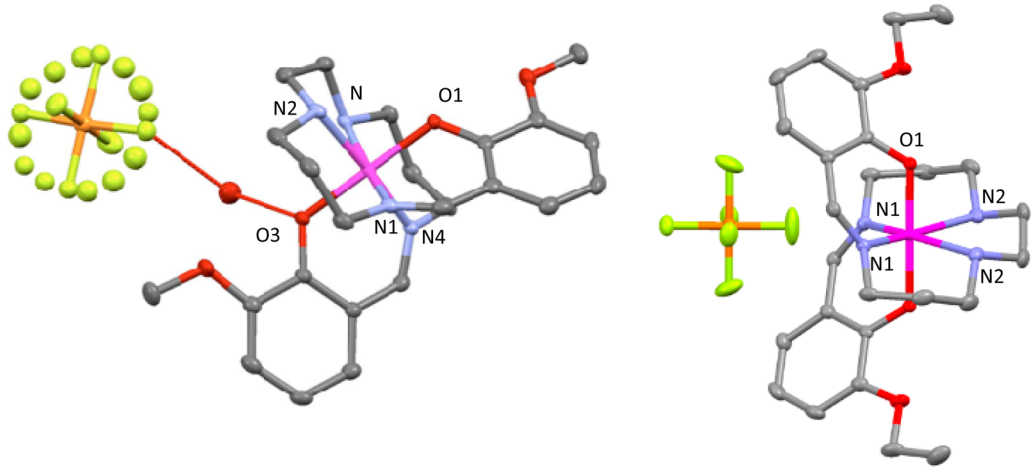

Figure 5. Hydrogen-bonding arrangement in [MnL1]PF_6·H_2O, (**1b**) (left) and illustration of "spinning top" PF_6^- counteranion and [MnL2]PF_6, (**2b**) (right) containing an ordered PF_6^- counteranion at 100 K.

dx.doi.org/10.1021/ic5003012 | *Inorg. Chem.* 2014, 53, 6022−6033

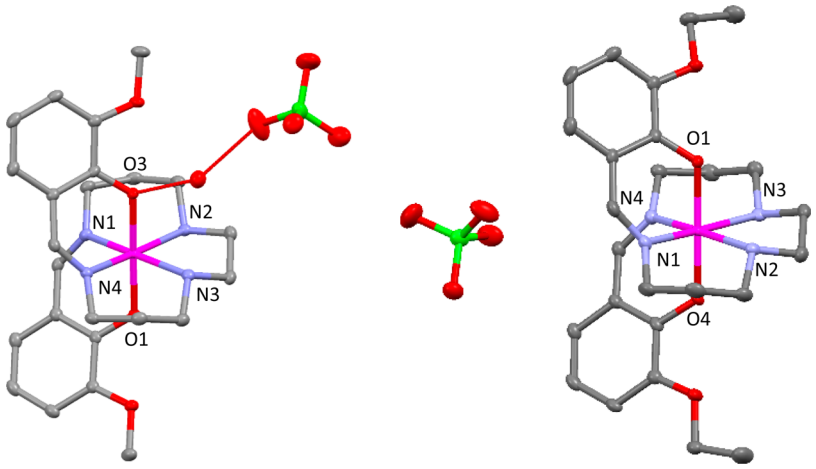

Figure 6. View of hydrogen-bonding interactions of $[MnL1]ClO_4 \cdot H_2O$, (**1c**) (left) at 100 K, and complex $[MnL2]ClO_4$, (**2c**) (right) at 100 K.

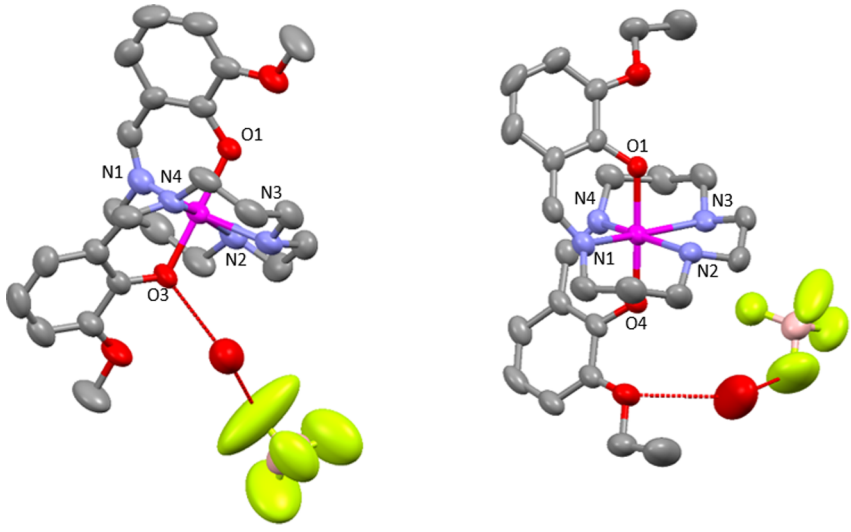

Figure 7. View of hydrogen-bonding interactions of $[MnL1]BF_4 \cdot H_2O$, (**1d**) (left) and $[MnL2]BF_4 \cdot 0.4H_2O$, (**2d**) (right) at 293 K.

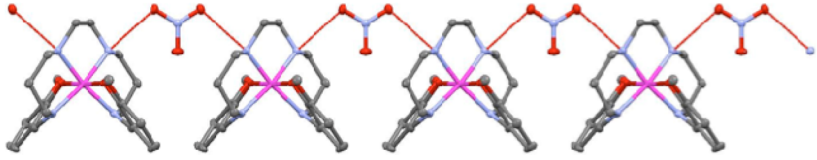

Figure 8. View of 1D hydrogen-bond chain of $[MnL1]NO_3$, (**1e**), at 100 K.

show direct hydrogen bonding to the alkoxy substituent, and this interaction persists upon heating to 293 K.

There are two distinct packing patterns for the NO_3^--containing complexes $[MnL1]NO_3$, (**1e**),[41] and $[MnL2]NO_3 \cdot EtOH$, (**2e**), due to the complexes having a difference in solvation. Complex (**1e**) forms one-dimensional (1D) chains resulting from one of the nitrate oxygen atoms hydrogen-bonding to the amine backbone, N_{amine}, of each of two adjacent cations, Figure 8. This 1D hydrogen chain is not disrupted upon warming to room temperature, even though the $Mn-N_{amine}$ distances increased during SCO.

Complex (**2e**) initially crystallized with an ethanol solvate in the crystal lattice in the first structure determination at 100 K. This results in a different packing arrangement within the lattice compared with the structure of the less hydrated (**2e′**), which was determined at 293 K some months later. At 100 K the structure of $[MnL2]NO_3$, (**2e**), contains discrete intermolecular hydrogen bonds from the ethanol solvate to the nitrate anion, which also forms a hydrogen bond with the amine backbone of the cation, Figure 9.

The hydrogen bond from the nitrate counterion to the amine backbone exists at both recorded temperatures of 100 and 293 K; however, the complex $[MnL2]NO_3 \cdot 0.6H_2O$, (**2e′**), at 293 K contains a disordered EtOH molecule, which was modeled with occupancy 0.6. As the electron density could not easily be modeled the Platon SQUEEZE program was used to compensate for the spread electron density.

Solution Studies. The electronic state of SCO complexes in solution does not always correspond to that in the solid state,[68] and therefore the spin state of all 10 complexes reported here was probed in acetonitrile using the Evans NMR method[69] and UV−vis absorption spectroscopy. The spin state at room temperature in acetonitrile solution was initially established via NMR,

dx.doi.org/10.1021/ic5003012 | Inorg. Chem. 2014, 53, 6022−6033

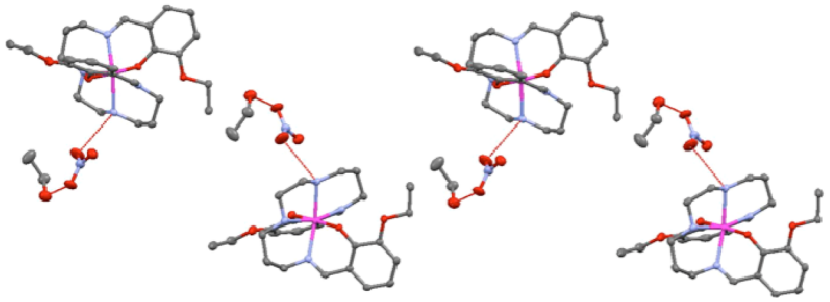

Figure 9. View of hydrogen-bonding interactions of $[MnL2]NO_3{\cdot}EtOH$, (**2e**), at 100 K.

Table 1, which indicates that all of the complexes are intermediate between HS and LS at room temperature. In contrast the solid-state SQUID data indicate a HS state for (**1a**), (**2a**), (**1b′**), (**2b**), and a high percentage of HS sites in the other complexes, Figure 1. However, the presence of both HS and LS states in acetonitrile solution at room temperature would help to explain the electronic absorption spectra shown in Figure 10 and

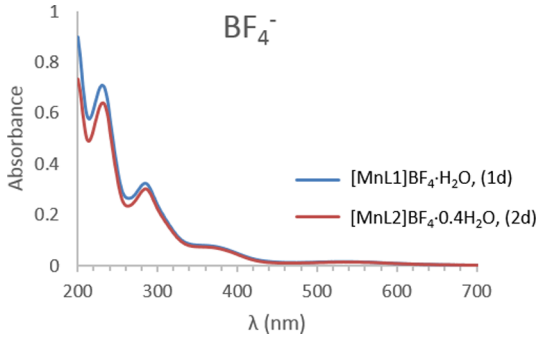

Figure 10. Electronic absorption spectra of $[MnL1]BF_4$, (**1d**), and $[MnL2]BF_4$ solvation of $0.4H_2O$, (**2d**).

Supporting Information, Figure S11, which suggest the presence of two electronic states.

The UV−vis spectra all show an absorption at approximately 380 nm, which is tentatively attributed to the HS component, and a more intense band at around 290 nm, assigned to the LS form. These are the first studies of SCO Mn^{III} complexes in solution and illustrate the ability of the ligand to stabilize the rare LS form of this ion in a noncrystalline environment. Work is underway to establish the changes in electronic absorption that accompany SCO in solution.

CONCLUSION

We reported solution and solid-state magnetic and structural properties of a series of 10 HS and SCO salts of complexes $[MnL1]^+$ and $[MnL2]^+$, where L1 and L2 are hexadentate Schiff-base ligands. The BPh_4^- salts of both L1 and L2 were HS between 10 and 280 K, whereas the PF_6^-, ClO_4^-, BF_4^-, and NO_3^- salts of both complex cations exhibit gradual SCO behavior, although none are fully HS at the upper temperature limit of the measurement. The influence of solvent is apparent in two complexes (**1b**) and (**2e**) changing profile upon loss of a full or partial solvate molecule, and the lability of spin state in solution was apparent from the NMR and UV−vis studies. The extra CH_2 group on the substituent in L2 is observed empirically to have the effect of increasing $T_{1/2}$ toward room temperature in the solid state. Further experimental and theoretical work is currently ongoing to expand our R-$Sal_2$323 series and to establish the prevalence of SCO for Mn(III) with this ligand system. This will be invaluable in attempting to design an SCO complex with a $T_{1/2}$ at room temperature for device applications.

EXPERIMENTAL SECTION

Instrumental details are described in the Supporting Information. Industrial methylated spirits (IMS) used instead of pure ethanol. MeCN is acetonitrile.

Complex (1a): $[MnL1]BPh_4$. To a well-stirred solution of *N*,*N*′-bis(3-aminopropyl)ethylenediamine (0.174 g, 1 mmol) in ethanol/MeCN (1:1 v/v, 10 mL) was added 3-methoxy-2-hydroxybenzaldehyde (0.304 g, 2.0 mmol) in ethanol/MeCN (1:1 v/v, 10 mL) by gravity filtration. The solution was stirred at room temperature for a further 10 min, after which time a solution of manganese(II) nitrate hydrate (0.179 g, 1 mmol) in ethanol/MeCN (1:1 v/v, 10 mL) was added; the solution changed from yellow to deep brown and was stirred for 10 min, after which time sodium tetraphenylborate (0.342 g, 1 mmol) was added to the solution. Stirring was continued for 10 min, and the product crystallized by slow evaporation of solvent. (0.121 g, 15%). IR (cm^{-1}): 3234 (w, sh), 2916 (w, sh), 1621 (st, sh), 1556 (w), 1439 (m, sh), 1252 (st, sh), 1 082 (st, sh), 983 (w), 850 (m, sh), 705 (st, sh).

Elemental Analysis: $C_{48}H_{52}BMnN_4O_4$. Theory: C: 67.08 H: 5.63 N: 6.80%. Actual: C: 67.03 H: 5.64 N: 6.82%.

Complex (2a): $[MnL2]BPh_4$. 3-Ethoxy-2-hydroxybenzaldehyde (0.166 g, 1 mmol) was dissolved in a 50:50 mixture of MeCN/IMS (10 mL). To this *N*,*N*′-bis(3-aminopropyl)ethylenediamine (0.087 g, 0.5 mmol) was added in a 50:50 mixture of MeCN/IMS (10 mL) by gravity filtration, and the solution was stirred for 15 min, yielding a yellow solution. Manganese(II) nitrate hydrate (0.089 g, 0.5 mmol) was then added, and the solution was stirred for 15 min. Sodium tetraphenylborate (0.171 g, 0.5 mmol) was then added directly, and the solution was stirred for 1 h, yielding a dark solution. This solution was then filtered into a clean dry beaker and allowed to crystallize. (0.228 g, 45.6%). IR (cm^{-1}): 3233 (w, sh), 3053 (w, sh), 2980 (w, sh) 1619 (st, sh), 1595 (w), 1462 (m, sh), 1252 (st, sh), 1077 (st, sh), 906 (w), 706 (st, sh).

Elemental Analysis: $C_{50}H_{56}BMnN_4O_4$. Theory: C 71.26 H 6.70 N 6.65%. Found: C 71.23 H 6.67 N 6.72%.

Complex (1b): $[MnL1]PF_6{\cdot}H_2O$. To a well-stirred solution of *N*,*N*′-bis(3-aminopropyl)ethylenediamine (0.174 g, 1 mmol) in ethanol/MeCN (50:50 v/v, 10 mL), a solution of 3-methoxy-2-hydroxybenzaldehyde (0.304 g, 2 mmol) dissolved in ethanol/MeCN (50:50 v/v, 10 mL) was added by gravity filtration. The solution was allowed to stir at room temperature for a further 10 min, after which time a solution of manganese(II) nitrate hydrate (0.179 g, 1 mmol) in 10 mL of ethanol/MeCN (50:50 v/v, 10 mL) was added dropwise by gravity filtration. During the addition, the solution changed to a deep brown color, and stirring continued for 10 min, after which time ammonium hexafluorophosphate (0.163 g, 1 mmol) was added to the solution. After a further 20 min of stirring, the solution was filtered by gravity filtration and allowed to stand overnight, during which crystals of X-ray quality were obtained (0.075 g, 13%). IR (cm^{-1}): 3467 (w, b), 2922 (w, sh), 1616 (st, sh), 1383 (m, sh), 1251 (st, sh), 1081 (m, sh), 841 (st, sh), 558 (w, sh).

Elemental Analysis: $C_{24}H_{34}F_6MnN_4O_5P$. Theory: C: 43.78 H: 5.21 N: 8.51%. Actual: C: 43.74 H: 5.14 N: 8.42%.

dx.doi.org/10.1021/ic5003012 | *Inorg. Chem.* 2014, 53, 6022−6033

Complex (2b): [MnL2]PF_6. 3-Ethoxy-2-hydroxybenzaldehyde (0.166 g, 1 mmol) was dissolved in a 50:50 mixture of MeCN/IMS (10 mL). To this, a solution of *N*,*N*′-bis(3-aminopropyl)ethylenediamine (0.087 g, 0.5 mmol) dissolved in a 50:50 mixture of MeCN/IMS (10 mL) was added by gravity filtration and allowed to stir for 15 min, yielding a yellow solution. Manganese(II) nitrate hydrate (0.089 g, 0.5 mmol) dissolved in a 50:50 mixture of MeCN/IMS (10 mL) was then added by gravity filtration and allowed to stir for 5 min. Ammonium hexafluorophosphate (0.082 g, 0.5 mmol) was then added directly, and the solution was stirred for 1 h, yielding a dark solution. This solution was then filtered into a clean dry beaker and allowed to crystallize. Dark crystals/powders were recovered (0.139 g, 40.4%). IR (cm^{-1}): 3484 (w, b), 2980 (w, sh), 1618 (st, sh), 1445 (m, sh), 1282 (st, sh), 1079 (m, sh), 843 (st, sh), 558 (w, sh).

Elemental Analysis: $C_{26}H_{36}F_6MnN_4O_4P$. Theory: C 46.71 H 5.43 N 8.38%. Found: C 46.57 H 5.33 N 8.43%.

Complex (1c): [MnL1]ClO_4·H_2O. A yellow-colored solution of 3-hydroxy-2-methoxybenzaldehyde (0.304 g, 2.0 mmol) dissolved in a 50/50 mixture of MeCN/IMS (20 mL) was filtered into a solution of *N*,*N*′-bis(3-aminopropyl)ethylenediamine (0.174 g, 1.0 mmol) in MeCN/IMS (50:50 v/v, 10 mL). This bright yellow-colored solution was stirred at room temperature for 30 min. Manganese(II) perchlorate hexahydrate (0.364 g, 1.0 mmol) was added to the reaction. A deep brown solution resulted, and the reaction was stirred at room temperature for a further 20 min, after which time the solution was gravity filtered. A first crop precipitated out of solution as brown crystals, which were filtered off and washed with a small amount of dichloromethane (0.262 g, 42.74%). IR (cm^{-1}): 3484 (b), 3264 (w), 3214 (w), 2921 (m, sh), 2857 (m, sh), 1618 (st, sh), 1078 (st, sh)

Elemental Analysis: $C_{24}H_{34}ClMnN_4O_9$. Theory: C 47.03 H 5.59 N 9.14%. Found: C 46.61 H 5.46 N 8.96%.

Complex (2c): [MnL2]ClO_4. 3-Ethoxy-2-hydroxybenzaldehyde (0.166 g, 1 mmol) was dissolved in a 50:50 mixture of MeCN/IMS (10 mL). To this, a solution of *N*,*N*′-bis(3-aminopropyl)ethylenediamine (0.087 g, 0.5 mmol) dissolved in a 50:50 mixture of MeCN/IMS (10 mL) was added by gravity filtration and allowed to stir for 15 min, yielding a yellow solution. Manganese(II) perchlorate hexahydrate (0.181 g, 0.5 mmol) dissolved in a 50:50 mixture of MeCN/IMS (10 mL) was then added by gravity filtration and allowed to stir for 1 h, yielding a dark solution. This solution was then filtered into a clean dry beaker and allowed to crystallize (0.077 g, 24.7%). IR (cm^{-1}): 3254 (w, b), 2974 (w, sh), 1619 (st, sh), 1386 (m, sh), 1282 (st, sh), 1098 (m, sh), 840 (st, sh), 621 (w, sh)

Elemental Analysis: $C_{26}H_{36}ClMnN_4O_8$. Theory: C 50.13 H 5.87 N 8.99%. Found: C 49.71 H 5.88 N 8.92%.

Complex (1d): [MnL1]BF_4·H_2O. To a well-stirred solution of *N*,*N*′-bis(3-aminopropyl)ethylenediamine (0.174 g, 1 mmol) in methanol/MeCN (50:50 v/v, 10 mL), a solution of 3-methoxy-2-hydroxybenzaldehyde (0.304 g, 2 mmol) in methanol/MeCN (50:50 v/v, 10 mL) was added by gravity filtration. The solution was stirred at room temperature for a further 10 min, after which time a solution of manganese(II) nitrate hydrate (0.179 g, 1 mmol) in 10 mL of methanol/MeCN (50:50 v/v, 10 mL), was added. During the addition, the solution changed to a deep brown color; stirring was continued for 10 min, after which time sodium tetrafluoroborate (0.104 g, 1 mmol) was added to the solution. After a further 10 min of stirring, the solution was filtered by gravity filtration, and crystals were collected (0.105 g, 14%). IR (cm^{-1}): 3568 (w, b), 2922 (w, sh), 2360 (w), 1619 (st, sh), 1470 (st, sh), 1277 (st, sh), 1051 (st, sh), 853 (m, sh), 750 (m, sh), 632 (m, sh).

Elemental Analysis: $C_{24}H_{34}BF_4MnN_4O_5$. Theory: C: 48.02 H: 5.71 N: 9.33%. Actual: C: 47.69 H: 5.61 N: 9.64%.

Complex (2d): [MnL2]BF_4·0.4H_2O. 3-Ethoxy-2-hydroxybenzaldehyde (0.166 g, 1 mmol) was dissolved in a 50:50 mixture of MeCN/IMS (10 mL). To this, a solution of *N*,*N*′-bis(3-aminopropyl)ethylenediamine (0.087 g, 0.5 mmol) dissolved in a 50:50 mixture of MeCN/IMS (10 mL) was added by gravity filtration and allowed to stir for 15 min, yielding a yellow solution. Manganese(II) nitrate hydrate (0.089 g, 0.5 mmol) dissolved in a 50:50 mixture of MeCN/IMS (10 mL) was then added by gravity filtration and stirred for 5 min. Ammonium tetrafluoroborate (0.052 g, 0.5 mmol) was then added directly, and the solution was stirred for 1 h. This solution was then filtered into a clean dry beaker and allowed to crystallize (0.123 g, 47.0%). IR (cm^{-1}): 2970 (w, b), 2870 (w, sh), 1619 (st, sh), 1575 (m, sh), 1245 (st, sh), 1080 (m, sh), 865 (st, sh), 634 (w, sh).

Elemental Analysis: $C_{26}H_{36.82}BF_4MnN_4O_{4.4}$. Theory: C 50.54 H 6.01 N 9.07%. Found: C 50.62 H 5.82 N 9.41%.

Complex (1e): [MnL1]NO_3. Neat *N*,*N*′-bis(3-aminopropyl)ethylenediamine (0.54 g, 3.1 mmol) was added to a solution of 3-methoxy-2-hydroxy-benzaldehyde (0.99 g, 6.5 mmol) in ethanol (25 mL), and then solid manganese(II)nitrate hydrate (0.54 g, 3 mmol) was added. The solution was heated to reflux for 20 min and filtered while hot. Black crystals formed almost instantly on cooling (0.65 g, 39%). IR (cm^{-1}): 3071 (w, b), 2928 (w, sh), 1618 (st, sh), 1384 (m, sh).

Elemental Analysis: $C_{24}H_{32}MnN_5O_7$. Theory: C 51.71 H 5.79 N 12.56%. Found: C 51.67 H 5.75 N 12.52%.

Complex (2e): [MnL2]NO_3·EtOH. Neat *N*,*N*′-bis(3-aminopropyl)-ethylenediamine (0.174 g, 1 mmol) was added to a solution of 3-ethoxy-2-hydroxy-benzaldehyde (0.332 g, 2 mmol) in a 50:50 mixture of MeCN/IMS (25 mL), and then solid manganese(II) nitrate hydrate (0.179 g, 1 mmol) was added after 15 min. The resulting brown solution was stirred for 1 h and then filtered. Black crystals formed upon evaporation of solvent (0.22 g, 34%). IR (cm^{-1}): 3527 (w, b), 2976 (w, sh), 1621 (st, sh), 1383 (m, sh).

Elemental Analysis: $C_{28}H_{42}MnN_5O_8$. Theory: C 53.25 H 6.70 N 11.09%. Found: C 53.19 H 6.64 N 11.03%.

■ ASSOCIATED CONTENT

Supporting Information

Magnetic data, X-ray experimental procedure, CCDC codes, ^1H NMR spectra, UV−vis spectra, and other data. This material is available free of charge via the Internet at http://pubs.acs.org.

■ AUTHOR INFORMATION

Corresponding Author

*E-mail: grace.morgan@ucd.ie.

Author Contributions

Authors B.G. and M.M.H. contributed equally.

Notes

The authors declare no competing financial interest.

■ ACKNOWLEDGMENTS

We thank the Science Foundation of Ireland for generous support via Investigator Project Award (12/IP/1703 to G.G.M) and a Walton Fellowship (11/W.1/I1954 to A.P). The award of a Government of Ireland Research Scholarship from the Irish Research Council for Science Engineering and Technology (IRCSET) (to B.G.) is gratefully acknowledged, as is the award of a National University of Ireland Travelling Scholarship (to M.H.) and a postgraduate studentship from Meath County Council (to L.G.). Significant funding for a SQUID magnetometer by the Irish Higher Education Authority is also gratefully acknowledged, as is a studentship (to C.A.M.) from the same agency under the PRTLI(III) program. All authors acknowledge the generous support of University College Dublin.

■ REFERENCES

(1) Gütlich, P.; Gaspar, A.; Garcia, Y. *Beilstein J. Org. Chem.* **2013**, *9*, 342−391.

(2) Rotaru, A.; Dugay, J.; Tan, R. P.; Guralskiy, I. y. A.; Salmon, L.; Demont, P.; Carrey, J.; Molnár, G.; Respaud, M.; Bousseksou, A. *Adv. Mater.* **2013**, *25*, 1745−1749.

(3) Bousseksou, A.; Molnár, G.; Salmon, L.; Nicolazzi, W. *Chem. Soc. Rev.* **2011**, *40*, 3313−3335.

(4) Bonhommeau, S.; Guillon, T.; Daku, L. M. L.; Demont, P.; Costa, J. S.; Létard, J.-F.; Molnár, G.; Bousseksou, A. *Angew. Chem., Int. Ed.* **2006**, *45*, 1625−1629.
(5) Matsuda, M.; Tajima, H. *Chem. Lett.* **2007**, *36*, 700−701.
(6) Gütlich, P.; Garcia, Y.; Goodwin, H. A. *Chem. Soc. Rev.* **2000**, *29*, 419−427.
(7) Gütlich, P.; Garcia, Y.; Spiering, H. *Magnetism: Molecules to Materials IV;* Miller, J. S., Drillon, M., Eds.; Wiley-VCH: Weinheim, Germany, 2003; pp 271−344.
(8) Fisher, D. C.; Drickamer, H. G. *J. Chem. Phys.* **1971**, *54*, 4825−37.
(9) Slichter, C. P.; Drickamer, H. G. *J. Chem. Phys.* **1972**, *56*, 2142−60.
(10) Ksenofontov, V.; Spiering, H.; Schreiner, A.; Levchenko, G.; Goodwin, H. A.; Gütlich, P. *J. Phys. Chem. Solids* **1999**, *60*, 393−399.
(11) Gütlich, P.; Ksenofontov, V.; Gaspar, A. B. *Coord. Chem. Rev.* **2005**, *249*, 1811−1829.
(12) Antonangeli, D.; Siebert, J.; Aracne, C. M.; Farber, D. L.; Bosak, A.; Hoesch, M.; Krisch, M.; Ryerson, F. J.; Fiquet, G.; Badro, J. *Science* **2011**, *331*, 64−67.
(13) Molnär, G.; Niel, V.; Real, J.-A.; Dubrovinsky, L.; Bousseksou, A.; McGarvey, J. J. *J. Phys. Chem. B* **2003**, *107*, 3149−3155.
(14) Qi, Y.; Müller, E. W.; Spiering, H.; Gütlich, P. *Chem. Phys. Lett.* **1983**, *101*, 503−5.
(15) Bousseksou, A.; Negre, N.; Goiran, M.; Salmon, L.; Tuchagues, J. P.; Boillot, M. L.; Boukheddaden, K.; Varret, F. *Eur. Phys. J. B* **2000**, *13*, 451−456.
(16) Bousseksou, A.; Varret, F.; Goiran, M.; Boukheddaden, K.; Tuchagues, J.-P. *Top. Curr. Chem.* **2004**, *235*, 65−84.
(17) Garcia, Y.; Kahn, O.; Ader, J.-; Buzdin, A.; Meurdesoif, Y.; Guillot, M. *Phys. Lett. A* **2000**, *271*, 145−154.
(18) McGarvey, J. J.; Lawthers, I. *J. Chem. Soc., Chem. Commun.* **1982**, 906−907.
(19) Hayami, S.; Gu, Z.- Z.; Shiro, M.; Einaga, Y.; Fujishima, A.; Sato, O. *J. Am. Chem. Soc.* **2000**, *122*, 7126−7127.
(20) Hauser, A. *Top. Curr. Chem.* **2004**, *234*, 155−198.
(21) Halcrow, M. A. *Chem. Soc. Rev.* **2008**, *37*, 278−289.
(22) Gütlich, P. *Top. Curr. Chem.* **2004**, *234*, 231−260.
(23) Vankó, G.; Renz, F.; Molnár, G.; Neisius, T.; Kárpáti, S. *Angew. Chem., Int. Ed.* **2007**, *46*, 5306−5309.
(24) Ono, K.; Yoshizawa, M.; Akita, M.; Kato, T.; Tsunobuchi, Y.; Ohkoshi, S.-I.; Fujita, M. *J. Am. Chem. Soc.* **2009**, *131*, 2782−2783.
(25) Ma, H.; Petersen, J. L.; Young, V. G., Jr.; Yee, G. T.; Jensen, M. P. *J. Am. Chem. Soc.* **2011**, *133*, 5644−5647.
(26) Venkataramani, S.; Jana, U.; Dommaschk, M.; Sönnichsen, F. D.; Tuczek, F.; Herges, R. *Science* **2011**, *331*, 445−448.
(27) Gütlich, P.; Hauser, A.; Spiering, H. *Angew. Chem., Int. Ed.* **1994**, *33*, 2024−54.
(28) Gütlich, P. *Struct. Bonding (Berlin, Ger.)* **1981**, *44*, 83−195.
(29) Real, J. A.; Gaspar, A. B.; Niel, V.; Muñoz, M. C. *Coord. Chem. Rev.* **2003**, *236*, 121−141.
(30) Kitchen, J. A.; Brooker, S. *Coord. Chem. Rev.* **2008**, *252*, 2072−2092.
(31) Van Koningsbruggen, P. J.; Maeda, Y.; Oshio, H. *Top. Curr. Chem.* **2004**, *233*, 259−324.
(32) Nihei, M.; Shiga, T.; Maeda, Y.; Oshio, H. *Coord. Chem. Rev.* **2007**, *251*, 2606−2621.
(33) Halcrow, M. A. *Chem. Soc. Rev.* **2011**, *40*, 4119−4142.
(34) Griffin, M.; Shakespeare, S.; Shepherd, H. J.; Harding, C. J.; Létard, J.-F.; Desplanches, C.; Goeta, A. E.; Howard, J. A. K.; Powell, A. K.; Mereacre, V.; Garcia, Y.; Naik, A. D.; Müller-Bunz, H.; Morgan, G. G.; Symmetry-Breaking Spin-State, A. *Angew. Chem., Int. Ed.* **2011**, *50*, 896−900.
(35) Hayami, S.; Komatsu, Y.; Shimizu, T.; Kamihata, H.; Lee, Y. H. *Coord. Chem. Rev.* **2011**, *255*, 1981−1990.
(36) Brooker, S.; Plieger, P. G.; Moubaraki, B.; Murray, K. S. *Angew. Chem., Int. Ed.* **1999**, *38*, 408−410.
(37) Hayami, S.; Kato, K.; Komatsu, Y.; Fuyuhiro, A.; Ohba, M. *Dalton Trans.* **2011**, *40*, 2167−2169.
(38) Hayami, S.; Urakami, D.; Kojima, Y.; Yoshizaki, H.; Yamamoto, Y.; Kato, K.; Fuyuhiro, A.; Kawata, S.; Inoue, K. *Inorg. Chem.* **2010**, *49*, 1428−1432.
(39) Halepoto, D. M.; Holt, D. G. L.; Larkworthy, L. F.; Leigh, G. J.; Povey, D. C.; Smith, G. W. *J. Chem. Soc., Chem. Commun.* **1989**, 1322.
(40) Sim, P. G.; Sinn, E. *J. Am. Chem. Soc.* **1981**, *103*, 241−3.
(41) Morgan, G. G.; Murnaghan, K. D.; Müller-Bunz, H.; McKee, V.; Harding, C. J. *Angew. Chem., Int. Ed.* **2006**, *45*, 7192−7195.
(42) Martinho, P. N.; Gildea, B.; Harris, M. M.; Lemma, T.; Naik, A. D.; Müller-Bunz, H.; Keyes, T. E.; Garcia, Y.; Morgan, G. G. *Angew. Chem., Int. Ed.* **2012**, *51*, 12597−12601.
(43) Pandurangan, K.; Gildea, B.; Murray, C.; Harding, C. J.; Müller-Bunz, H.; Morgan, G. G. *Chem.—Eur. J.* **2012**, *18*, 2021−2029.
(44) Gildea, B.; Gavin, L. C.; Murray, C. A.; Müller-Bunz, H.; Harding, C. J.; Morgan, G. G. *Supramol. Chem.* **2012**, *24*, 641−653.
(45) Gandolfi, C.; Cotting, T.; Martinho, P. N.; Sereda, O.; Neels, A.; Morgan, G. G.; Albrecht, M. *Dalton Trans.* **2011**, *40*, 1855−1865.
(46) Murray, C. A. Geometric and Lattice Influences in Jahn−Teller Ions. PhD Thesis, University College Dublin: Dublin, Ireland, 2007.
(47) Wang, S.; Ferbinteanu, M.; Marinescu, C.; Dobrinescu, A.; Ling, Q.-D.; Huang, W. *Inorg. Chem.* **2010**, *49*, 9839−9851.
(48) Chen, Y.; Cao, F.; Wei, R. M.; Zhang, Y.; Zhang, Y. Q.; Song, Y. *Dalton Trans.* **2014**, *43*, 3783−3791.
(49) Quesada, M.; Prins, F.; Bill, E.; Kooijman, H.; Gamez, P.; Roubeau, O.; Spek, A. L.; Haasnoot, J. G.; Reedijk, J. *Chem.—Eur. J.* **2008**, *14*, 8486−8499.
(50) Yamada, M.; Hagiwara, H.; Torigoe, H.; Matsumoto, N.; Kojima, M.; Dahan, F.; Tuchagues, J.-P.; Re, N.; Iijima, S. *Chem.—Eur. J.* **2006**, *12*, 4536−4549.
(51) Dîrtu, M. M.; Rotaru, A.; Gillard, D.; Linares, J.; Codjovi, E.; Tinant, B.; Garcia, Y. *Inorg. Chem.* **2009**, *48*, 7838−7852.
(52) Leita, B. A.; Neville, S. M.; Halder, G. J.; Moubaraki, B.; Kepert, C. J.; Létard, J.-F.; Murray, K. S. *Inorg. Chem.* **2007**, *46*, 8784−8795.
(53) Hostettler, M.; Törnroos, K. W.; Chernyshov, D.; Vangdal, B.; Bürgi, H.-B. *Angew. Chem., Int. Ed.* **2004**, *43*, 4589−4594.
(54) Kitchen, J. A.; White, N. G.; Jameson, G. N. L.; Tallon, J. L.; Brooker, S. *Inorg. Chem.* **2011**, *50*, 4586−4597.
(55) Conti, A. J.; Chadha, R. K.; Sena, K. M.; Rheingold, A. L.; Hendrickson, D. N. *Inorg. Chem.* **1993**, *32*, 2670−80.
(56) Kennedy, B. J.; McGrath, A. C.; Murray, K. S.; Skelton, B. W.; White, A. H. *Inorg. Chem.* **1987**, *26*, 483−495.
(57) Djukic, B.; Poddutoori, P. K.; Dube, P. A.; Seda, T.; Jenkins, H. A.; Lemaire, M. T. *Inorg. Chem.* **2009**, *48*, 6109−6116.
(58) Djukic, B.; Dube, P. A.; Razavi, F.; Seda, T.; Jenkiins, H. A.; Britten, J. F.; Lemaire, M. T. *Inorg. Chem.* **2009**, *48*, 699−707.
(59) Sertphon, D.; Harding, D. J.; Harding, P.; Murray, K. S.; Moubaraki, B.; Cashion, J. D.; Adams, H. *Eur. J. Inorg. Chem.* **2013**, *2013*, 788−795.
(60) Nielsen, P.; Toftlund, H.; Bond, A. D.; Boas, J. F.; Pilbrow, J. R.; Hanson, G. R.; Noble, C.; Riley, M. J.; Neville, S. M.; Moubaraki, B.; Murray, K. S. *Inorg. Chem.* **2009**, *48*, 7033−7047.
(61) Galet, A.; Gaspar, A. B.; Muñoz, M. C.; Real, J. A. *Inorg. Chem.* **2006**, *45*, 4413−4422.
(62) Drew, M. G. B.; Harding, C. J.; McKee, V.; Morgan, G. G.; Nelson, J. *J. Chem. Soc., Chem. Commun.* **1995**, 1035−8.
(63) Guionneau, P.; Marchivie, M.; Bravic, G.; Létard, J.-F.; Chasseau, D. *Top. Curr. Chem.* **2004**, *234*, 97−128.
(64) Pritchard, R.; Barrett, S. A.; Kilner, C. A.; Halcrow, M. A. *Dalton Trans.* **2008**, 3159−3168.
(65) Gandolfi, C.; Morgan, G. G.; Albrecht, M. *Dalton Trans.* **2012**, *41*, 3726−3730.
(66) Kahn, O. *Molecular Magnetism;* Wiley-VCH: Weinheim, Germany, 1993; p 10.
(67) Marchivie, M.; Guionneau, P.; Létard, J.-F.; Chasseau, D. *Acta Crystallogr., Sect. B* **2005**, *61*, 25−28.
(68) Shores, M. P.; Klug, C. M.; Fiedler, S. R. *Spin-State Switching in Solution, in Spin-Crossover Materials: Properties and Applications;* Halcrow, M. A., Ed.; John Wiley & Sons, Ltd.: Oxford, U.K., 2013. doi: 10.1002/9781118519301.ch10.
(69) Evans, D. F. *J. Chem. Soc.* **1959**, 2003−2005.